Journal of Magnetism and Magnetic Materials 487 (2019) 165313

Contents lists available at ScienceDirect

Journal of Magnetism and Magnetic Materials

journal homepage: www.elsevier.com/locate/jmmm

Research articles

Hierarchical structure and the origins of coercivity in exchange-coupled Co-Pt nanochessboards

J.A. Floro[a,*], E.P. Vetter[a], P. Ghatwai[a], L.D. Geng[b], Y.M. Jin[b], W.A. Soffa[a]

[a] University of Virginia, Department of Materials Science and Engineering, United States
[b] Michigan Technological University, Department of Materials Science and Engineering, United States

ABSTRACT

We report the first detailed investigation into how exchange-coupled magnetic properties evolve during the formation of the Co-Pt $L1_0 + L1_2$ nanochessboards, which self-assemble by a pseudo-spinodal mechanism below the eutectoid isotherm. The maximum observed coercivities exceed 3 kOe, but these values are more than 5 times lower than the largest values predicted by micromagnetics simulations of ideal, single-colony chessboards. For magnetization reversal controlled by nucleation, a simple analysis readily reconciles this discrepancy by accounting for misorientation associated with the polycrystalline structure that exists at the 50 μm lengthscale, demagnetizing fields associated with eutectoid colonies at the 0.5 μm lengthscale, and non-idealities in the chessboard structure at the tiling lengthscale of about 20 nm.

1. Introduction

In 1991, Leroux, et al., published a detailed electron microscopy study of a fascinating "nanochessboard" structure that formed spontaneously during thermal treatment of a Co-Pt alloy [1]. Shown schematically in Fig. 1(a), the nanochessboard consists of a quasi-periodic, 2 + 1D array of ordered $L1_0$ nanorods embedded in an ordered $L1_2$ matrix. The chessboard formally results from eutectoid decomposition, $A1 \rightarrow L1_0 + L1_2$, where the eutectoid composition is about 60 at% Pt. The microstructure differs from the more typical lamellar eutectoid structure, e.g., pearlite, since it derives from disorder/order transformations wherein the product phases inherit the crystalline orientation of the parent phase, and the resulting heterointerfaces are therefore coherent. For phase compositions near the crossover point in Gibbs free energy, i.e., where $G_{L10} = G_{A1}$, the phase transformation can be "pseudo-spinodal" as suggested by Ni and Khachaturyan [2], wherein $L1_0$ forms in the A1 matrix, requiring only a small initial composition fluctuation. Subsequently, the phase compositions continuously evolve, followed by $L1_2$ ordering in the cubic phase. The tetragonal transformation strain establishes the pattern formation and orientation selection that ultimately results in the nanochessboard [3,4].

Despite the fact that CoPt $L1_0$ is a well-studied ferromagnet with very high magnetocrystalline anisotropy, the magnetic properties of the Co-Pt nanochessboard remained unknown for the two decades following its discovery. In particular, since Co-rich $L1_2$ is a soft (low magnetocrystalline anisotropy) ferromagnet, the chessboard is especially intriguing in the context of exchange-coupled ferromagnetism. Exchange coupling between a magnetically hard phase and a magnetically soft phase can provide a beneficial combination of coercivity and remanent magnetization [5,6]. The lengthscales associated with the hard and soft phases critically determine the degree of coupling. Exchange coupling and closely related exchange spring magnetism have been extensively investigated in planar epitaxial thin films, pertinent to magnetic recording media. Films offer quasi-1D geometry with directly controllable layer thicknesses that facilitate or modify exchange-coupling behavior [7]. On the other hand, in bulk materials, solid-state nanostructuring and phase separation approaches provide nanocrystalline composites in 3D. In these materials exchange coupling is inherently complex, subject to locally varying coupling and interactions, grain orientations, particle size distributions, and phase morphology. The nanochessboard offers a different paradigm for examining exchange-coupling mechanisms – produced in bulk by solid-state transformation, with a simplified periodic geometry, appropriate lateral lengthscales, and fully coherent heterophase interfaces.

The nanochessboard features a hierarchy of structural, chemical and magnetic lengthscales, see both Fig. 1 (schematic) and Fig. 2 (actual). The material produced by casting bulk Co-Pt alloys will be polycrystalline A1, with grain sizes of order 20–50 μm. Appropriate aging in the $L1_0 + L1_2$ two-phase region will promote chessboard formation within each grain. Intragranular chessboards form in colonies, distinguished by the particular choice of the three ⟨1 0 0⟩ directions in the parent A1 lattice that is parallel to the nanorod axes, see Figs. 1(b) and 2(b). The colony lengthscale will typically be of order 200–500 nm. The chessboard tile size and spacing occurs on the 10–30 nm lengthscale,

* Corresponding author.
E-mail address: jaf9r@virginia.edu (J.A. Floro).

https://doi.org/10.1016/j.jmmm.2019.165313
Received 10 February 2019; Received in revised form 30 April 2019; Accepted 15 May 2019
Available online 22 May 2019
0304-8853/

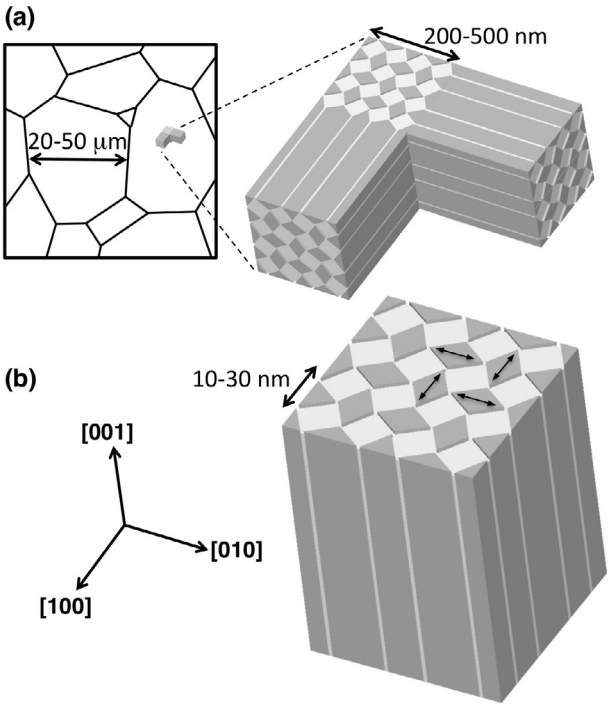

Fig. 1. (a) Each grain of the bulk polycrystal contains chessboard colonies arranged along the three ⟨1 0 0⟩ axes of the parent grain. The idealized colony arrangement is shown at right. (b) A portion of a singe colony, showing the arrangement of darker $L1_0$ "tiles" amidst the lighter $L1_2$ matrix. The orientations of the $L1_0$ c-axes, which are also the magnetic easy axes, are shown with the smaller black arrows. The hierarchy of structural dimensions is indicated.

and can be controlled via process conditions, see Fig. 2(b). Finally, chemical ordering in the $L1_0$ and $L1_2$ phases occurs at the atomic scale, dictating the saturation magnetization and magnetocrystalline anisotropy.

Our previous work examined how the tiling lengthscale affected exchange coupling between the hard $L1_0$ and soft $L1_2$ phase [8,9]. The chessboard tile size and periodicity were controlled by the cooling rate through the eutectoid isotherm, and exchange interactions between the hard and soft phases could be varied from partial to complete coupling.

In this paper, we show how the hierarchical structure impacts the observed coercivity through orientation effects, heterogeneity, and demagnetizing fields. We first show data on the evolution of the chessboard ordering during aging. This allows us to identify peak hardness samples. We previously used micromagnetic simulations to investigate the magnetization and reversal behavior in single-colony chessboard structures, as a function of the tile size [10]. The coercivities predicted using micromagnetics are much larger than the observed coercivities, even at peak hardness. This could imply that either the magnetic parameters used in the calculation were incorrect, or that micromagnetics fails to capture the relevant physics. However, here we will combine the micromagnetics results with a simple analytical model to show that the simulation values can in fact provide reasonable agreement with experimental data by considering the polycrystalline nature, and hierarchy of structural lengthscales, within our specimens.

2. Experimental details

Bulk binary Co-Pt alloys were processed by arc melting high purity Co (99.9%) and Pt (99.99%) in an argon atmosphere, to produce approximately 70 g melts. The alloy composition was 59.8 ± 0.1 at% Pt, which we will refer to as $Co_{40}Pt_{60}$. This was determined by dissolving 25 mg alloy samples in 4 ml of hot aqua regia and then using Inductively Coupled Plasma – Optical Emission Spectroscopy (ICP-OES). The alloys were alternately rolled and homogenized/recrystallized by thermal annealing to attain a final plate thickness of 300–400 μm. Prior to thermal annealing, samples were encapsulated in quartz tubes that were evacuated and then back-filled with argon, and then sealed off with a hydrogen torch. The homogenizing/recrystallizing treatment was conducted either at 925 °C for 8 h, or 975 °C for 24 h, followed by water quenching to retain the disordered FCC phase. This A1-phase starting material will be referred to henceforth as the "base material". No significant differences directly attributable to the different homogenization treatments were observed.

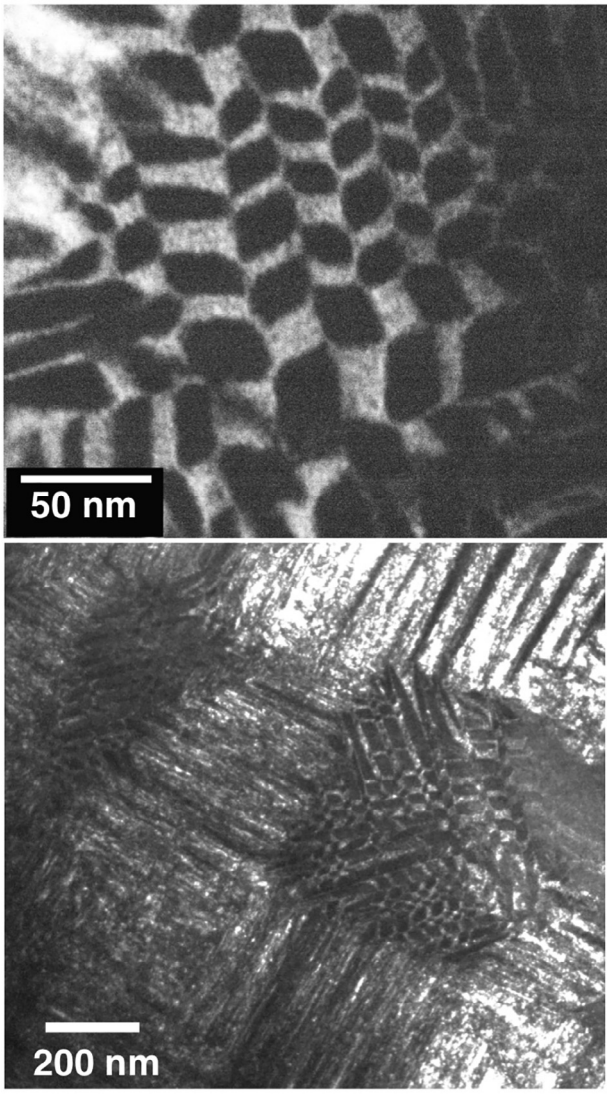

Fig. 2. (1 1 0) Transmission electron dark field micrographs, {0 0 1} zone axis, from sample 600C/0W. (a) Chessboard colony viewed along the nanorod axis. (b) Lower magnification, but same imaging conditions as (a), showing multiple equiaxed colonies in all three equivalent ⟨1 0 0⟩ orientations.

Multiple pieces were cut from the base material, encapsulated, and annealed to promote eutectoid decomposition to form the chessboard structure. The most common annealing regimen was to first heat the samples to 750 °C (nominally within the A1 region of the phase diagram), where they were held for 30 min. Then the samples were continuously cooled at a rate of either 40 °C/day or 80 °C/day, from 750 °C to a final temperature, T_f. A subsequent isothermal annealing for a time, t_{iso}, was sometimes performed at T_f prior to water quenching and removal from the ampoule. We will sometimes refer to specific samples in the format T_f/t_{iso}, where t_{iso} will be in days, e.g., "600C/7D". Whenever t_{iso} = 0D, this implies that the material was quenched immediately

upon reaching T_f.

X-ray diffraction (XRD) was used for phase identification, where, after an initial scan across the range 2θ = 15–90°, slower scans at the minimum goniometer step size were performed over the {1 0 0}, {2 0 0} and {3 1 1} reflections. Confirmation of the chessboard microstructure was obtained from transmission electron microscopy (TEM) in select samples.

Vibrating sample magnetometry (VSM) using a Lakeshore Cryotronics Model 7400 VSM was performed to determine the room temperature magnetic response on disk-shaped samples 3 mm in diameter and 150 μm thick. The external field was applied in the plane of the disks to minimize demagnetizing fields. Samples were typically field demagnetized, then M-H loops were obtained to H = ± 2 T using a step size of 250 Oe and an averaging time of 0.5 s. We analyze the initial magnetization curve, the major loop, and the first derivative of the major loop, dM/dH, which will be referred to as the instantaneous susceptibility.

3. Results

In order to identify peak hardness samples during chessboard processing, we performed thermal aging studies. Fig. 3(a) summarizes the thermal processing conditions used in this work. An effective timescale is used, where $t_{eff} = 0$ corresponds to T = 730 °C, the nominal eutectoid temperature established by Leroux, et al. [1]. That is, time is only counted while the samples are undercooled with respect to the eutectoid. Fig. 4 shows the M vs. H loops and the corresponding instantaneous susceptibilities, dM/dH, for the samples cooled through the eutectoid isotherm at 40 °C per day (green circles in Fig. 3(a)). Fig. 5 is similar to Fig. 4, but compares only 600C/0D and 600C/8D samples

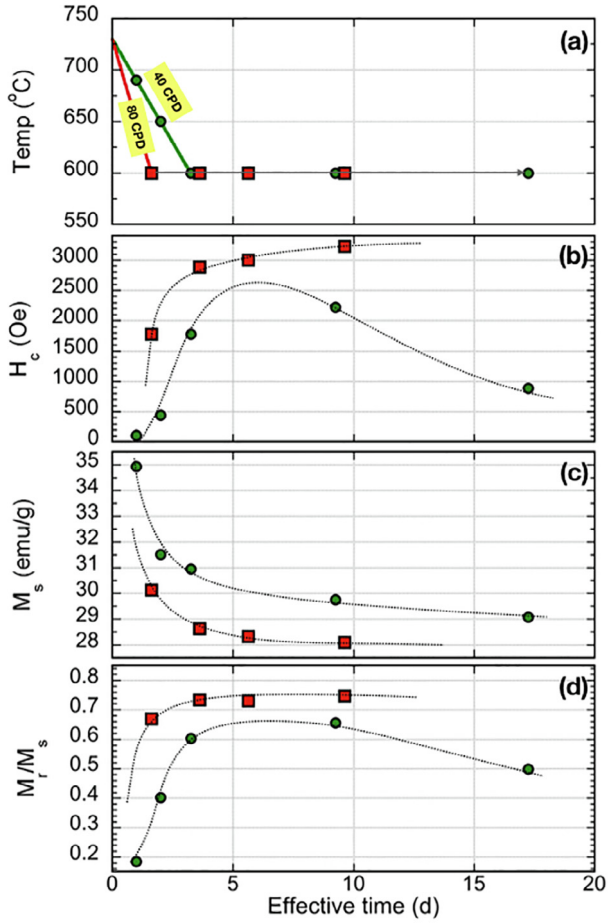

Fig. 3. (a) Thermal process conditions used herein. Green circles were cooled at 40 °C/day, while red squares were cooled at 80 °C day. (b) – (d) show the coercivity, saturation magnetization, and remanence ratio during aging. Dotted lines are guides to the eye. (For interpretation of the references to colour in this figure legend, the reader is referred to the web version of this article.)

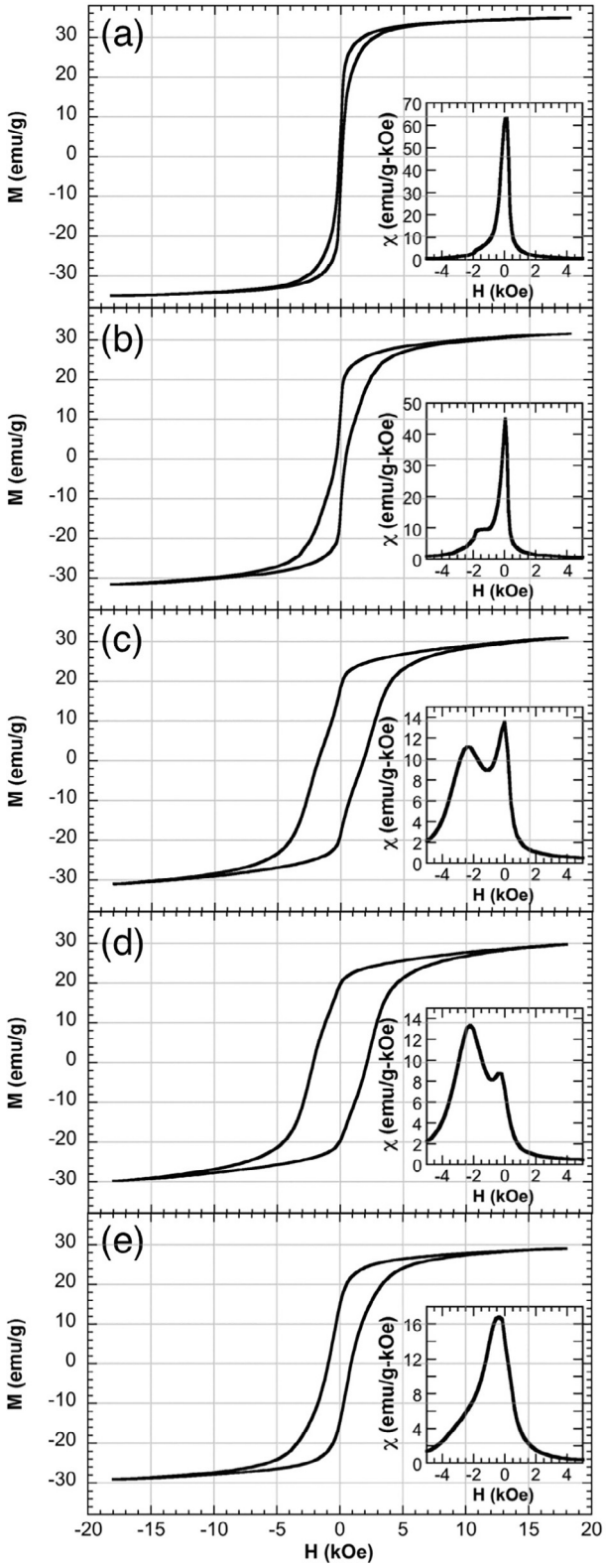

Fig. 4. M vs. H loops for samples cooled at 40°/day: (a) 690C/0D, (b) 650C/0D, (c) 600C/0D, (d) 600C/7D, and (e) 600C/14D. Shown inset are the instantaneous susceptibilities, plotted only over a limited range of applied field during the sweep from positive to negative saturation.

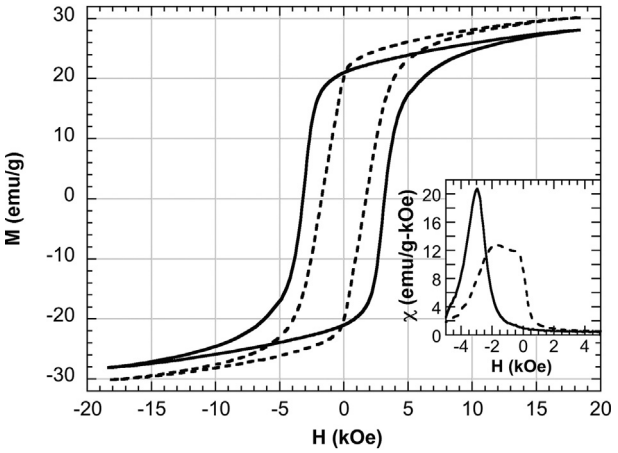

Fig. 5. M vs. H loops for samples cooled at 80˚/day, comparing 600C/0D with 600C/8D. Shown inset are the instantaneous susceptibilities, plotted only over a limited range of applied field during the sweep from positive to negative saturation.

cooled at 80˚/day. From the hysteresis loops we obtain the coercivity (H_c), the saturation magnetization (M_s), remnant magnetization (M_r) and the remanence ratio, M_r/M_s. These are summarized in Fig. 3(b)–(d).

The magnetic aging behavior can be summarized as follows. Coercivity increases as the samples are undercooled relative to the eutectoid isotherm. At 40 ˚C/day cooling rate, a maximum coercivity in the vicinity of 2500 Oe is reached. Concomitantly, the remanence ratio obtains a maximum value of 0.67. For the higher cooling rate of 80 ˚C/day, the coercivity and remanence ratios are enhanced, reaching 3200 Oe and 0.75, respectively. While overaging is clearly observed at 40 ˚C/day, aging times for the 80 ˚C/day samples were insufficient to produce a clear maximum in H_c and M_r/M_s. In both sets of samples, the saturation magnetization monotonically decreases, consistent with ongoing chemical ordering [11].

The progressive formation of the magnetically hard $L1_0$ phase from a soft-phase background is evident in Fig. 4. A peak at larger |H| is clearly discernable in the susceptibility after cooling to 650 ˚C and quenching (sample 650C/0D in Fig. 4(b)), corresponding to regions of the sample with higher coercive fields. Additional aging increases both the volume fraction and coercive field of the $L1_0$ phase, see Fig. 4(c) and (d). Overaging is readily apparent in the sample heated isothermally for 2 weeks, Fig. 4(e). The data for the 80 ˚C/day samples is rather different, see Fig. 5. While the least-annealed sample shows indications of hard and soft phases, all longer isothermal anneals are found to produce only a single, hard magnetic peak.

The maximum remanence ratios observed in Fig. 3(d) for the 40 ˚C/day and 80 ˚C/day samples range from 0.67 to 0.75, indicating that exchange coupling is likely occurring between the $L1_0$ and $L1_2$ (or residual A1) phases. The M(H) and dM/dH data in Fig. 4 clearly identify the presence of two magnetic phases that are switching quasi-independently, implying that exchange coupling is incomplete. These results have also been supplemented using first order reversal curve (FORC) analysis, and some of these results have been published elsewhere [8,9]. A key result is that the samples processed at 80 ˚C/day exhibit only a single magnetic phase, while XRD shows that two magnetic phases are present, and TEM confirms the chessboard configuration. Hence at 80 ˚C/day, complete exchange coupling of the $L1_0$ and $L1_2$ phases was achieved, whereas at 40 ˚C/day, only partial coupling of the soft-phase occurred due to the longer lengthscales.

Although the Co-Pt nanochessboard was first reported in 1991, X-ray diffraction measurements of Co-Pt nanochessboards have never been published. XRD results are included here to support the progression of phase formation in the chessboard, in concert with the magnetic properties reported above.

Fig. 6 compares XRD scans of the {1 0 0} superlattice and {2 0 0} fundamental reflections from all the samples cooled at 40 ˚C/day in Fig. 3(a). Results for the {3 1 1} fundamental reflection are similar to those for the {2 0 0}. The results for processing chessboards at 80 ˚C/day are quite similar to those processed at 40 ˚C/day. Diffraction spectra in Fig. 6 were normalized by the maximum intensity, and each scan was vertically offset in the plot for clarity. The raw data smoothed with 5-point boxcar to reduce noise, which improves clarity and does not change peak positions or lineshapes. At the bottom of Fig. 6, reflections from Co-Pt samples with compositions on either side of the

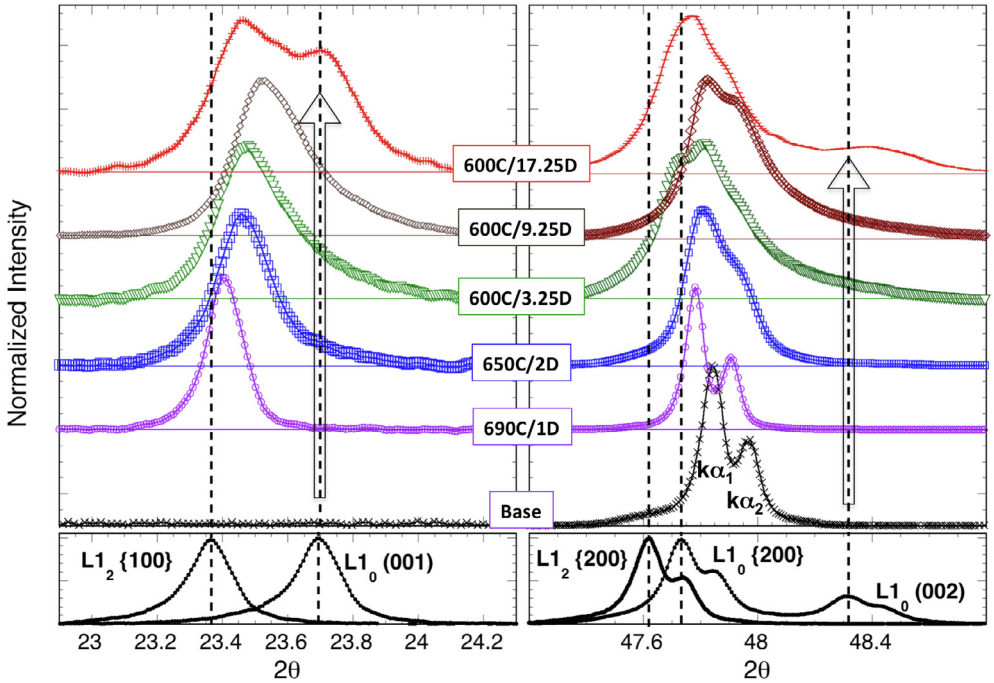

Fig. 6. X-ray diffraction spectra from the base material, and the samples cooled at 40˚/day. Left panels show the {1 0 0} reflection, while right panels show the {2 0 0} reflection. Spectra from separate phase-pure samples are shown at the bottom. Aging times are effective times as shown in Fig. 3(a).

$L1_0 + L1_2$ coexistence region are shown. These nominally phase-pure samples serve as calibration standards for the two-phase materials. For the A1 base material no superlattice reflection was observed and the {2 0 0} peak is symmetric.

One surprising observation is that in the least-aged samples, e.g., 690C/0W, there is already a prominent {1 0 0} diffraction peak associated with $L1_2$. This is unexpected from considerations of the chessboard formation process, but this could result if sample first passed through the A1 + $L1_2$ coexistence region, rather than directly through the eutectoid. Preliminary calorimetric studies support this hypothesis.

Examination of Fig. 6 shows that the subsequent formation of the tetragonal $L1_0$ phase from the A1/$L1_2$ matrix is indicated by the increasing positive skew of the {1 0 0} and {2 0 0} Bragg reflections, associated with the emergence of the (0 0 1) and (0 0 2) peaks of $L1_0$, respectively. The block arrows in the figure highlight the $L1_0$ evolution. Separate peaks for the ordered phases are only resolved for the over-aged 600C/2W chessboard, presumably relating not only to complete ordering, but perhaps also phase coarsening such that the "true" lattice parameters manifest in regions that are mechanically less constrained by neighboring phases.

In principle, peak fitting or Rietveld refinement could be performed to obtain lattice parameters, the chemical order parameters and the relative volume fractions of each phase [11]. However, these samples have nanoscale transformation lengthscales and triaxial coherency strains, leading to extensive peak shifts and overlaps. Such coherency strains are inherent to $L1_0$ ordering within a cubic (A1 or $L1_2$) matrix [2–4]. In addition, a paucity of data on how the $L1_0$ and $L1_2$ lattice parameters vary with both order parameter and composition (since phases in the chessboard are well off the ideal stoichiometries) frustrates quantitative analysis. Taken together, this results in excessive uncertainty in peak fitting or refinement, and all attempts failed due to a lack of internal self-consistency. Nonetheless, a qualitative interpretation of the structural phase evolution readily emerges that is fully consistent with the evolution of the magnetic properties.

4. Discussion

The magnetic data and XRD spectra reveal the continuous evolution of the magnetically hard $L1_0$ phase from a soft magnetic matrix with aging below the eutectoid isotherm. TEM further shows that this process is associated with self-assembly into the chessboard microstructure. As the chessboards form, the remanence ratio increases concomitantly with the coercivity, where for processing at 40 °C/day, M_r/M_s reaches a maximum of 0.67. This is consistent with weak to moderate exchange coupling associated with chessboard tiling lengthscales in the range of 25–40 nm. For processing at 80 °C/day, the remanence ratio reaches 0.75, indicative of more complete coupling. In a prior paper we used FORC, TEM and micromagnetic simulations to demonstrate the evolution from partial to complete exchange-coupling as the tiling lengthscales were reduced within the nanochessboards [8]. This is consistent with estimates of the critical coupling lengthscale from Kneller and Hawig, $\delta = 2\pi\ (A/2K)^{1/2} = 18$ nm, where K is the uniaxial anisotropy constant and A is the exchange coupling coefficient [5]. This calculation uses $K_1 = 1 \times 10^7$ erg/cm^3 determined for the fully-ordered $L1_0$ phase at this composition and $A = 2.5 \times 10^{-6}$ erg/cm [11].

The micromagnetics simulations described in detail elsewhere predict coercivities in chessboards as a function of the chessboard lengthscale [10]. A summary of the predicted coercive fields is shown in Fig. 7, where the magnetic field is applied along the [1 0 0], [1 1 0] and [0 0 1] directions. Importantly for this discussion, the predicted coercive fields are as high as 17 kOe. Such fields are much larger than the ~3 kOe maximum coercive fields obtained for real chessboards in Fig. 3(b). Note that the micromagnetic simulations, which are 2 + 1D and use periodic boundary conditions in the plane, effectively consider an extended, single-orientation chessboard. To assess how the real

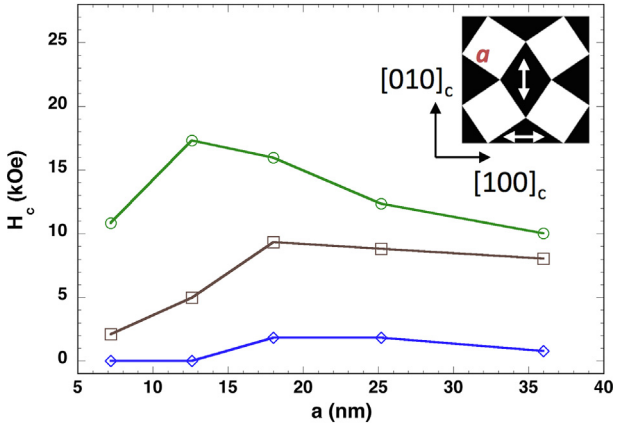

Fig. 7. Predicted coercivity of nanochessboards as a function of $L1_2$ tile size, "a" (see inset), from micromagnetics simulations. The external field is applied along [1 1 0] (green circles), [1 0 0] (brown squares) and [0 0 1] (blue diamonds). (For interpretation of the references to colour in this figure legend, the reader is referred to the web version of this article.)

microstructure modifies the observed coercivity in a simple but insightful fashion, treatments of the critical nucleation field by Kronmüller are used herein [12]. The assumption that nucleation determines the coercive field rather than domain wall pinning is justified on the basis of the micromagnetics simulations, where local rotations of the magnetization appear to be more important than extended domain formation and wall propagation. These results are further supported by Lorentz microscopy of chessboards, which show that $L1_0$ tiles form individual domains, and extended domain formation is not dominant [13,14].

Kronmüller [12] modified the classic expression for the nucleation field developed by Brown [15] as follows:

$$H_c = \alpha_\psi \alpha_K^{nuc} \left(\frac{2\langle K_1 \rangle}{\langle M_s \rangle} \right) - N_{eff} \langle M_s \rangle \quad (1)$$

The factor α_ψ accounts for varied orientations of the easy axis vs. the applied field. The factor α_K^{nuc} accounts for heterogeneities in the magnetocrystalline anisotropy where local reductions in K_1, e.g., at grain boundaries or voids, can locally reduce the nucleation field. Hence, both α_ψ and α_K^{nuc} are ≤ 1. The second term on the right is due to demagnetizing effects associated with free poles at surfaces or interfaces.

The *ideal* chessboard structure is inherently heterogeneous in K_1 due to the presence of the periodic hard $L1_0$ and soft $L1_2$ phases. Rather than attempting to estimate α_K^{nuc}, $< K_1 >$ and $< M_s >$ for the chessboard, we simply recognize that the intrinsic heterogeneities of the ideal chessboard are already captured in the micromagnetics simulations, thus

$$H_c^{MM} = \alpha_K^{nuc} \left(\frac{2\langle K_1 \rangle}{\langle M_s \rangle} \right) \quad (2)$$

where H_c^{MM} is the coercivity determined from micromagnetics, see Fig. 7.

We can now make a first estimate of the coercivity of a material that has randomly oriented grains, each containing chessboard colonies along the three ⟨1 0 0⟩ directions of the original A1 matrix. We take $\alpha_\psi = 0.5$, characteristic of random orientations, as shown by Stoner and Wohlfarth [16]. The demagnetizing factor arises from the presence of uncompensated poles at surfaces or interfaces. In our material, the most likely location for these poles is at the boundaries of each chessboard colony, where there is a discontinuity in the magnetic easy axes. While grain boundaries will also have free poles, the density of colony/colony interfaces is two orders of magnitude larger. Fig. 2(b) suggests

that colonies are roughly cube-shaped in external morphology, and should then have a demagnetizing factor of about 4 [17]. Taking $H_c^{MM} = 17$ kOe from Fig. 7, and the measured $< M_s > = 500$ emu/cm^3, Eq. (1) gives an estimate of the measured coercivity, $H_c = 6.5$ kOe. This is within a factor of about 2 of the value $H_c = 3$ kOe found in Fig. 3(b).

While this estimate already shows decent agreement, we can improve the analysis by acknowledging that real chessboards do not have ideal morphology, *cf.* Figs. 1 and 2. We can account for this by taking

$$H_c = \alpha_\psi \alpha'_K H_c^{MM} - N_{eff} \langle M_s \rangle, \quad (3)$$

where α_K' accounts for softening associated with distortions of the chessboard from the ideal, e.g. arising from locally coarsened chessboard tiles that are evident in Fig. 2. To obtain numerical agreement with $H_c = 3$ kOe requires $\alpha_K' = 0.59$ (all other values as before), which is eminently reasonable [12]. For example, $L1_2$ regions that are coarser than the average size will be more decoupled from the surrounding hard phase, and can readily nucleate reversed domains at lower fields. An alternative way to obtain numerical agreement would be to increase the demagnetizing factor, $N_{eff} > 4$. This can readily result from acute angles at the polygonal peripheries of grains or colonies. For example, Kronmüller plots for Nd-based magnets yield values as large as $N_{eff} = 7.2\pi$ [12].

This simple and intuitive analysis thus uses the full hierarchical structure, from atomic ordering to large grain matrix, combined with micromagnetics simulations of the ideal chessboard configuration, to reproduce the measured coercivity. The analysis also highlights the unsurprising fact that in order to obtain coercivities in excess of 10 kOe, growth of a single crystal or highly textured A1 starting material, combined with aging in an applied magnetic field to suppress colony formation, would be required.

5. Conclusions

We have reported the first detailed investigation into how the magnetic properties evolve during the formation of the Co-Pt nanochessboards. Exchange coupling depends on the tiling lengthscale of the chessboards, in agreement with micromagnetics simulations, and the lengthscale is controlled primarily by varying the continuous cooling rate through the eutectoid isotherm. Maximum coercivities of about 3 kOe are found during aging studies, and these values are more than 5× lower than the largest values predicted in micromagnetics for ideal, single-colony chessboards. For magnetization reversal controlled by nucleation, an analysis by Kronmüller can readily reconcile this discrepancy by accounting for misorientation associated with the polycrystalline structure that exists at the 50 μm lengthscale, demagnetizing fields associate with the interfaces between eutectoid colonies at the 0.5 μm lengthscale, and non-idealities in the chessboard structure at the tiling lengthscale of about 20 nm. All of this modifies the intrinsic nucleation field predicted by the micromagnetics for the exchange-coupled $L1_0 + L1_2$ phases in the quasi-periodic, 2 + 1D chessboard structures.

Acknowledgements

We gratefully acknowledge National Science Foundation support under grants DMR-1105336 and DMR-1709914 (UVA) and DMR-1409317 (MTU). We thank Helge Heinrich and Chris Duska for assistance with TEM, and assistance with specimen preparation by Wade Jensen. We benefited from discussions with Christine Leroux, Yann Le Bouar, and Jim Howe.

References

[1] C. Leroux, A. Loiseau, D. Broddin, G. Vantendeloo, Philos. Mag. B 64 (1991) 57.
[2] Y. Ni, A.G. Khachaturyan, Nature Mater. 8 (2009) 410.
[3] Y. Le Bouar, A. Loiseau, A.G. Khachaturyan, Acta Mater. 46 (1998) 2777.
[4] Y. Ni, Y.M. Jin, A.G. Khachaturyan, Acta Mater. 55 (2007) 4903.
[5] E.F. Kneller, R. Hawig, IEEE Trans. Magn. 27 (1991) 3588–3600.
[6] R. Skomski, J.M.D. Coey, Phys. Rev. B 48 (1993) 15812–15816.
[7] E.E. Fullerton, J.S. Jiang, S.D. Bader, J. Magn. Magn. Mater. 200 (1999) 392–404.
[8] E.P. Vetter, P. Ghatwai, W.A. Soffa, J.A. Floro, IEEE Magn. Lett. 6 (2015) 6600104.
[9] E.P. Vetter, L. Geng, P. Ghatwai, D.A. Gilbert, Y.M. Jin, W.A. Soffa, J.A. Floro, Appl. Phys. Lett. Mater. 4 (2016) 096103.
[10] L.D. Geng, W.A. Soffa, J.A. Floro, Y.M. Jin, J. Appl. Phys. 123 (2018) 093901.
[11] P. Ghatwai, E. Vetter, M. Hrdy, W.A. Soffa, J.A. Floro, J. Magn. Magn. Mater. 375 (2015) 87.
[12] H. Kronmüller, Micromagnetic background of hard magnetic materials, in: G.J. Long, F. Grandjean (Eds.), Supermagnets, Hard Magnetic Materials, Kluwer, 1991, pp. 461–498.
[13] I. Kashyap, Y.M. Jin, E.P. Vetter, J.A. Floro and M. De Graef, Microsc. Microanal. doi: 10.1017/S143192761800034X.
[14] I. Kashyap, E.P. Vetter, J.A. Floro, M. De Graef, J. Magn. Magn. Mater. 479 (2019) 204.
[15] W.F. Brown Jr., Rev. Mod. Phys. 17 (1945) 15.
[16] E.C. Stoner, E.P. Wohlfarth, Philos. Trans. R. Soc. Lond. A 240 (1948) 43.
[17] D.J. Dunlop, Geophys. Res. Lett. 10 (1983) 79.